The International Journal of Cardiovascular Imaging
https://doi.org/10.1007/s10554-024-03111-0

ORIGINAL PAPER

Inversion recovery and saturation recovery pulmonary vein MR angiography using an image based navigator fluoro trigger and variable-density 3D cartesian sampling with spiral-like order

Jason Craft[1] · Jonathan Weber[1] · Yulee Li[1] · Joshua Y. Cheng[1] · Nancy Diaz[1] · Karl P. Kunze[2] · Michaela Schmidt[3] · Marie Grgas[1] · Suzanne Weber[1] · John Tang[1] · Roosha Parikh[1] · Afiachukwu Onuegbu[1] · Ann-Marie Yamashita[1] · Elizabeth Haag[1] · Daniel Fuentes[4] · Michael Czipo[4] · Radhouene Neji[5] · Cristian B. Espada[1] · Leana Figueroa[1] · Jonathan A. Rothbaum[1] · Kana Fujikura[6] · Ruqiyya Bano[7] · Omar K. Khalique[1] · Claudia Prieto[5,8] · Rene M. Botnar[5,9]

Received: 16 November 2023 / Accepted: 7 April 2024

Abstract

Contrast enhanced pulmonary vein magnetic resonance angiography (PV CE-MRA) has value in atrial ablation pre-procedural planning. We aimed to provide high fidelity, ECG gated PV CE-MRA accelerated by variable density Cartesian sampling (VD-CASPR) with image navigator (iNAV) respiratory motion correction acquired in under 4 min. We describe its use in part during the global iodinated contrast shortage. VD-CASPR/iNAV framework was applied to ECG-gated inversion and saturation recovery gradient recalled echo PV CE-MRA in 65 patients (66 exams) using .15 mmol/kg Gadobutrol. Image quality was assessed by three physicians, and anatomical segmentation quality by two technologists. Left atrial SNR and left atrial/myocardial CNR were measured. 12 patients had CTA within 6 months of MRA. Two readers assessed PV ostial measurements versus CTA for intermodality/interobserver agreement. Inter-rater/intermodality reliability, reproducibility of ostial measurements, SNR/CNR, image, and anatomical segmentation quality was compared. The mean acquisition time was 3.58 ± 0.60 min. Of 35 PV pre-ablation datasets (34 patients), mean anatomical segmentation quality score was 3.66 ± 0.54 and 3.63 ± 0.55 as rated by technologists 1 and 2, respectively ($p = 0.7113$). Good/excellent anatomical segmentation quality (grade 3/4) was seen in 97% of exams. Each rated one exam as moderate quality (grade 2). 95% received a majority image quality score of good/excellent by three physicians. Ostial PV measurements correlated moderate to excellently with CTA (ICCs range 0.52–0.86). No difference in SNR was observed between IR and SR. High quality PV CE-MRA is possible in under 4 min using iNAV bolus timing/motion correction and VD-CASPR.

Claudia Prieto and Rene M. Botnar Senior both serve as senior authors.

✉ Jason Craft
Jason.Craft@chsli.org

[1] Division of Cardiovascular Imaging, DeMatteis Cardiovascular Institute, St Francis Hospital & Heart Center, 101 Northern Blvd, Greenvale, NY 11548, USA

[2] MR Research Collaborations, Siemens Healthcare Limited, Camberley, UK

[3] Siemens Healthineers, Erlangen, Germany

[4] Biosense Webster Incorporated, Irvine, CA, USA

[5] School of Biomedical Engineering and Imaging Sciences, King's College London, London, UK

[6] Division of Cardiology, NYU Grossman School of Medicine, New York, NY, USA

[7] Department of Nephrology and Hypertension, Stony Brook University Hospital, New York, NY 11794, USA

[8] School of Engineering, Pontificia Universidad Católica de Chile, Santiago, Chile

[9] Institute of Biological and Medical Engineering, Pontificia Universidad Católica de Chile, Santiago, Chile

Published online: 27 April 2024

Graphical Abstract

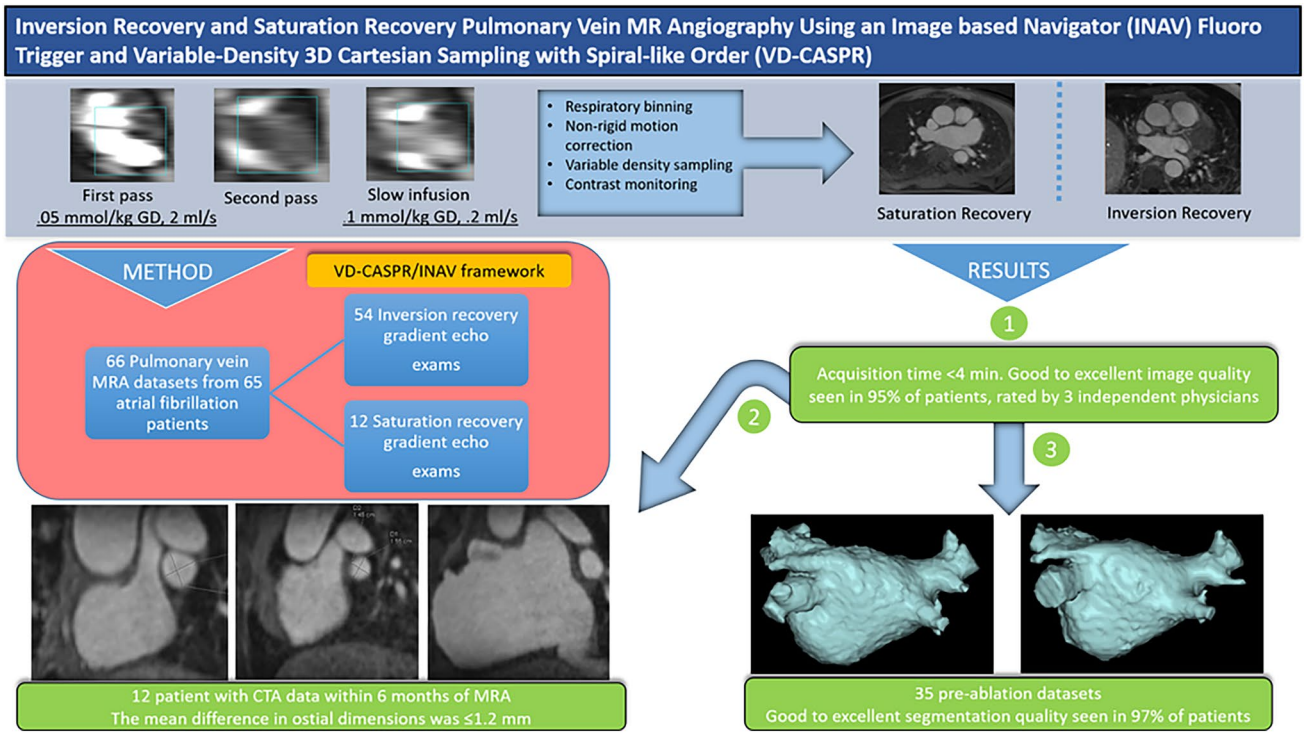

Keywords Magnetic resonance angiography · Atrial fibrillation · Left atrial delayed enhancement · Variable density cartesian sampling · Image based navigators

Abbreviations

bSSFP	Balanced steady-state free precession
CE-MRA	Contrast enhanced magnetic resonance angiography
CNR	Contrast to noise
CTA	Computed tomography angiography
dNAV	Diaphragmatic navigator
GBCA	Gadolinium based contrast agent
iNAV	Image based navigator
IPAT	Integrated parallel acquisition techniques
IR GRE	Inversion recovery gradient recalled echo
Dixon GRE	Inversion recovery Dixon gradient recalled echo
PV MRA	Pulmonary vein magnetic resonance angiography
MRA	Magnetic resonance angiography
MRI	Magnetic resonance imaging
LA	Left atrial
LGE	Late gadolinium enhancement
SNR	Signal to noise
SR GRE	Saturation recovery gradient recalled echo
VD-CASPR	Variable-density 3D Cartesian sampling with spiral-like order

Introduction

Recent shortages of iodinated contrast have highlighted the importance and role of magnetic resonance angiography (MRA) for pre-procedural imaging. In May, 2022, the Food and Drug Administration reported shortages of iohexol and iodixanol intraveneous contrast media products for computed tomography angiography (CTA) imaging [1]. This led to 2 months of rationing of iodinated contrast materials for use in critical non-elective procedures such as invasive coronary angiography. During this period, gadolinium-based contrast agents (GBCA) remained widely available. Several centers have used pulmonary vein MRA (PV MRA) for pre-ablation imaging, however, certain limitations exist depending on the acquisition strategy. Ungated first pass contrast enhanced MRA (CE-MRA) cannot effectively freeze cardiac motion and provides reduced quality of anatomical segmentation compared to PV CTA [2], and overall quality compared to respiratory gated PV MRA [3]. Registration of ungated first pass PV CE-MRA with 3D late gadolinium enhancement (LGE) is also compromised due to unsuppressed cardiac motion, differences in spatial location, and differences in spatial resolution. Non-contrast based 3D balanced

steady-state free precession (bSSFP) suffers from blood flow artifacts and off-resonance effects in the pulmonary veins and left atrium [4]. Although Magnetization transfer inversion recovery (MTC-BOOST) substantially reduces bSSFP artifacts and simultaneously provides dark blood images, the scan efficiency is reduced by a factor of 2 [5]. Likewise, Dixon GRE techniques (T2 prep, or combined T2 prep/IR prep [6]) have longer repetition times, potentially requiring the use of higher acceleration factors or larger temporal windows for a given acquisition length. This may result in increased spatial blurring.

The addition of cardiac gating to first pass CE-MRA improves visualization of certain structures, such as the aortic root, but motion suppression is still inferior to free breathing respiratory gated MRA [7]. Traditionally, a diaphragmatic navigator (dNAV) can provide the prerequisite respiratory gating; however, acquisition times are often long and unpredictable. An image navigator (iNAV) overcomes this limitation by directly providing estimation of respiratory motion for motion correction. Both 2D and 3D iNAV approaches have been utilized for motion correction [8–11]. Instead of tracking the diaphragmatic interface, the iNAV tracks structures such as the blood pool contrast of the heart, thereby avoiding the use of a motion model [12]. Therefore, a restrictive respiratory gating window (typically +/− 2.5–3 mm) is not needed, effectively resulting in 100% respiratory scan efficiency. 2D translational iNAV-derived motion profiles in the head-to-foot, and left-to-right directions can be extracted and estimated on a per cardiac cycle basis and is used to bin data with respect to respiration to the respective bin center. Once all data is collected, further inter-bin retrospective non-rigid motion correction is used to reconstruct the 3D dataset.

iNAV motion correction combined with variable-density 3D Cartesian sampling with spiral-like order (VD-CASPR) [13] and non-rigid motion corrected reconstruction has successfully been applied to 3D coronary MRA, 3D LGE, and non-contrast MRA [14–17], among others. However, the iNAV method requires relatively stable signal intensity of the left ventricular blood pool in order to facilitate proper tracking; rapid time-signal intensity variation results in tracking failure (supplemental_video_1). Stability of the blood pool signal can be quickly and efficiently achieved after the first and second pass of a small bolus injection of gadolinium based contrast agent (GBCA) with a continuous GBCA infusion providing T1 shortening during image acquisition (supplemental_video_2). However, GBCA transit time has significant subject to subject variation, and therefore direct observation of the first, second pass, and arrival of the continuous infusion provides subject specific timing for MRA scan initiation; avoids early scan initiation which may result in iNAV tracking failure; and late scan initiation which may miss the arrival of the continuous GBCA infusion. Here, we aim to utilize the aforementioned iNAV/VD-CASPR framework to enable free-breathing motion corrected 3D CE-MRA of the pulmonary veins at near isotropic spatial resolution within a short scan time, using iNAV as a monitoring tool to provide precision timing of the 3D CE-MRA scan window in relation to contrast agent bolus arrival.

Materials and methods

This was a single-center Institutional Review Board-approved study consisting of iNAV motion corrected PV MRA scans obtained as part of research or clinical protocols from March 2022 to November 2022. A flow chart of participant enrollment is provided in Fig. 1. 46 out of 65 patients' exams were performed during the May–July 2022 period coinciding with the global shortage of iodinated contrast. HIPAA-compliant research was performed in accordance with the Declaration of Helsinki. All studies were performed on a 1.5 T system (MAGNETOM Sola, Siemens Healthcare, Erlangen, Germany). For prospectively acquired studies, all 40 consecutively enrolled patients provided informed consent to publish de-identified data and medical images. Informed consent was waived by the same IRB for retrospective collection of additional 25 consecutively collected CMR exams. 12 patients had CTA exams performed within 6 months of MRA (mean 23 days, range 0–144 days); specifically 10 patients had CTA exams performed within 30 days or less of MRA (including 2 patients with both exams on the same day, 2 patients with both exams within 24 h, and 4 patients with both exams within 1 week). One patient had an interim PVI between imaging studies, with the MRA performed approximately 5 months subsequent to CTA and PVI.

Overview of CMR workflow and MRA protocol

The CMR protocol consisted of 3 long axis bSSFP cines, (4 chamber, 2 chamber, and 3 chamber), PV CE-MRA, and short axis bSSFP cines acquired in that order. To determine the highest (end expiratory) position of the left atrium, a coronal free breathing bSSFP scout was run over the course of 30 phases during free breathing. Typically, 80–88 axial slices were needed to encompass the pulmonary veins, left atrium, and left atrial appendage.

PV MRA was acquired using inversion or saturation recovery single echo gradient recalled echo (IR GRE, SR GRE). An overview of the pulse sequence acquisition is provided in Fig. 2. The VD-CASPR 3D acquisition pattern featured a golden angle rotation of spiral-like Cartesian k-space trajectory between successive cardiac cycles [13]. A total acceleration factor of 2.9 was used. K-space data was reconstructed using a non-rigid motion-compensated

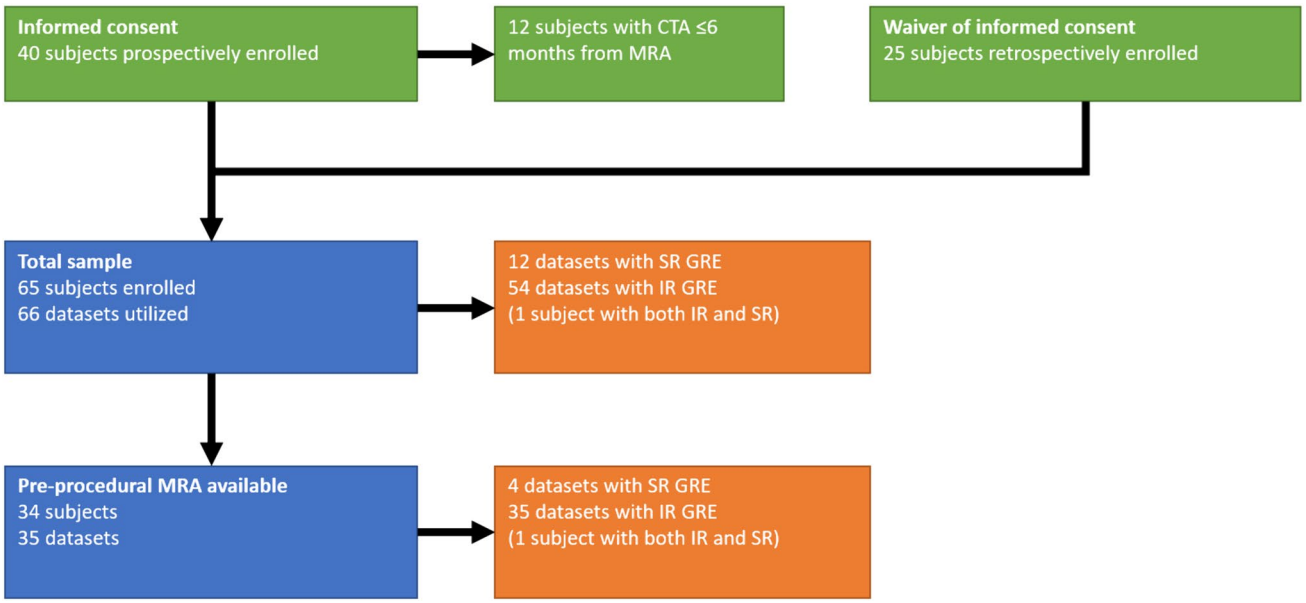

Fig. 1 Flow diagram of participant enrollment

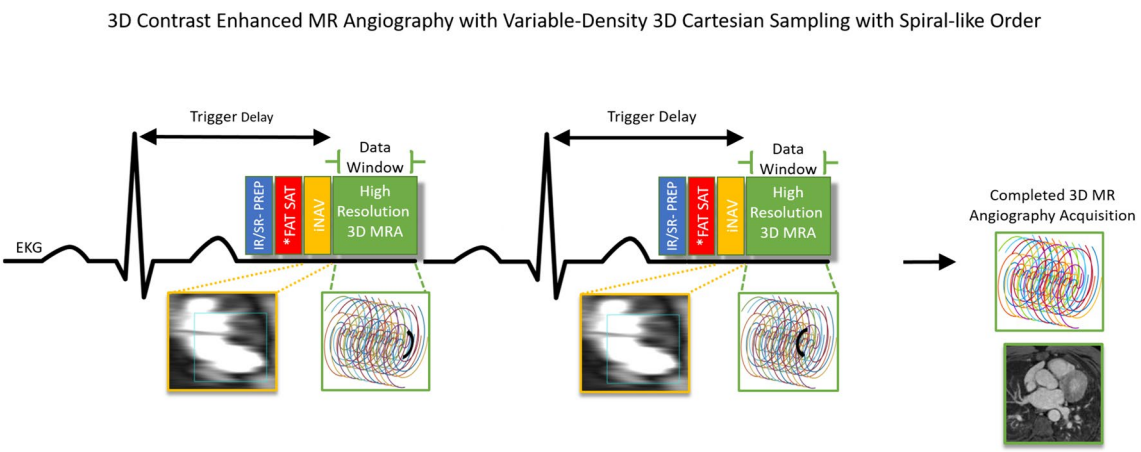

Fig. 2 Pulse sequence schematic for the contrast enhanced MR angiography featuring saturation (SR) or inversion recovery (IR) gradient echo readout; iNAV for joint estimation of respiratory motion in the head-foot, left–right directions with 100% scan efficiency; and alternating 3D spiral interleaves. Chemically shift selective fat saturation (*) is only used in conjunction with saturation recovery preparation

iterative 3D SENSE reconstruction implemented inline on the scanner [14].

Gating window selection and MRA setup

The cardiac rest periods were determined using free breathing 4 chamber bSSFP cine (35.9 ms temporal resolution) prior to CE-MRA. For patients with irregular rhythms (including atrial fibrillation), or ventricular rates of 80 BPM or higher, the systolic rest period of the lateral mitral valve annulus was selected. Otherwise, the diastolic rest period was selected. The data window duration was typically limited to 130 ms but further adjusted as needed to allow a maximum imaging time of 4 min for PV CE-MRA. This selection represented a tradeoff between residual cardiac motion, overall scan time, and duration of contrast infusion.

The iNAV and saturation band position (used to suppress signal from the arms for CE-MRA) was determined using free-breathing 3 plane localizers. The optimal position of the navigator was defined as covering the base of the left ventricle on the coronal localizer; avoiding the chest wall fat; and encompassing on the aortic root on the axial localizer while left/right centered on the left ventricle.

The imaging parameters for iNAV IR GRE, and SR GRE for pulmonary vein MRA are provided in Table 1. The inversion time selected for IR GRE was similar to previous studies [18, 19]; for systolic imaging, the value was adjusted to fit within the cardiac rest period. Additionally, for patients with cardiac devices, a 6000 Hz hyperbolic secant adiabatic wideband inversion recovery pulse was used, in conjunction with a center frequency offset of + 1500 Hz [20].

Contrast administration and iNAV fluoro trigger

With conventional linear or centric ordering, maximal T1 shortening can be targeted to the appropriate time to center of k-space. The spiral-like interleave reordering of the VD-CASPR sampling acquires central portions of k-space during each cardiac cycle throughout the acquisition length. The first and second pass of the bolus are only observed and not captured during CE-MRA acquisition. Therefore, giving the smallest bolus dose to facilitate tracking of the iNAV, while leaving the largest possible amount of remaining contrast for the plateau continuous dose was thought to give the best results. This also would provide the greatest flexibility in case of variable heart rates (atrial fibrillation) and/or missed vectorcardiogram triggers that could extend the acquisition duration longer than expected. A saline bolus following the contrast bolus was necessary for the contrast to clear the tubing (8 ml) completely.

A total of 0.15 mmol/kg of Gadobutrol (Gadavist™, Bayer Healthcare Pharmaceutical) was used per patient. 0.05 mmol/kg was used as the bolus dose, administered at 2 ml/s, followed by a saline bolus of 20 ml at the same rate. Immediately, a slow infusion dose of 0.1 mmol/kg at a rate of 0.2 ml/sec followed, with 20 ml of saline an identical rate.

Two identical copies (or program steps) of the iNAV 3D IR GRE or SR GRE sequence were present in the protocol; the first was triggered prior to contrast administration and functioned solely as a "fluoro trigger" to monitor the first pass, second pass, and continuous infusion passage. The second program step made identical to the first was triggered upon peak of the continuous infusion dose in the pulmonary artery (Fig. 3a), and immediately after stopping the first program step. Both iNAV 3D IR GRE and SR GRE sequences were triggered in the exact same fashion. The window level was adjusted as needed to visualize the three different components of contrast passage (Fig. 3a). Image reconstruction time was less than 2 min for each 3D dataset. Typical representative images for iNAV 3D IR GRE and SR GRE, are found in Figs. 4 and 5 respectively.

Measurement of SNR and CNR

A mid ventricular slice was selected for assessment of left atrial (LA) SNR and LA/myocardial CNR (LA $CNR_{myocardium)}$ in all pulmonary vein datasets. Circular regions of interest were included in the left atrium (20–30 mm^2) and myocardium; background region of interest typically included the entire space anterior to the chest wall. LA SNR was calculated as the mean signal in the left atrium divided by the mean background signal. LA $CNR_{myocardium}$ was calculated as the mean signal intensity difference between the left atrium and myocardium, divided by the mean background signal. All measurements were performed by a CMR physician with 10 years of experience (JC).

Table 1 3D whole heart iNAV based sequence parameters

Imaging parameters for pulmonary vein MRA		
Sequence	Inversion recovery GRE (PV MRA)	Saturation recovery GRE (PV MRA)
FOV	320 mm (axial)	320 mm (axial)
Spatial resolution	1.3 × 1.3 mm	1.3 × 1.3 mm
Slice thickness	1.4 mm	1.4 mm
Slice resolution	90%	90%
Fat Saturation	No	CHESS
Motion correction	iNAV	iNAV
Acceleration Factor	2.9	2.9
Bandwidth	579 Hz/px	579 Hz/px
Flip angle	18°	18°
TI/Saturation time	220–260 ms (systolic) 290 ms (diastolic)	150 ms
TE/TR	1.42 ms/3.89 ms	1.42 ms/3.89 ms
Data window duration	62–130 ms	62–130 ms

PV pulmonary vein; *MRA* magnetic resonance angiography; *GRE* gradient recalled echo; *FOV* field of view; *CHESS* chemically selective saturation; *iNAV* image navigator; *TE* echo time; *TR* repetition time

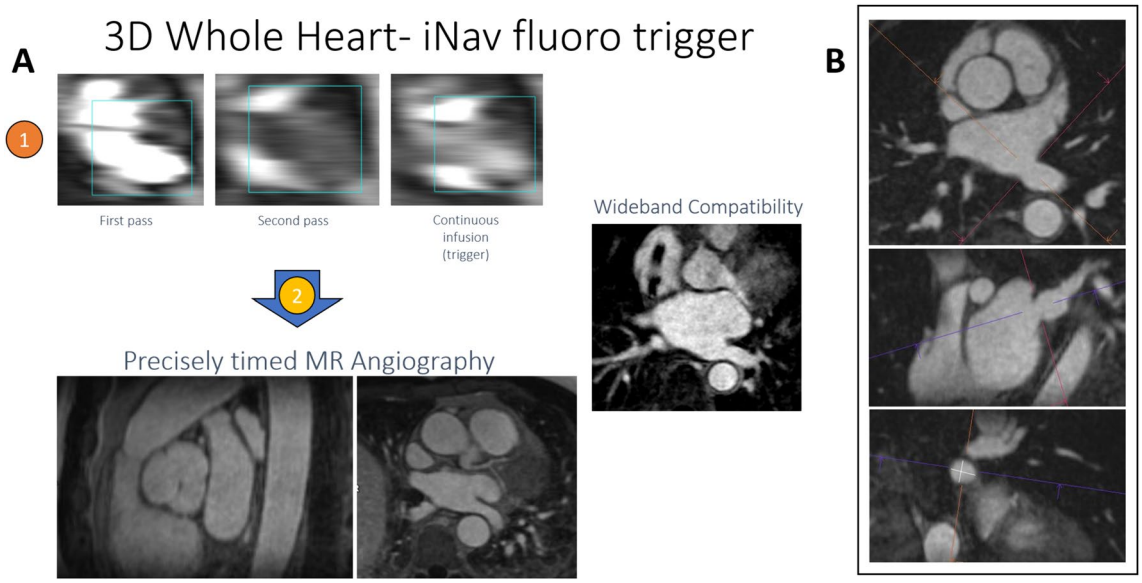

Fig. 3 **A** The image navigator (iNAV) fluoro trigger method for MR angiography. Two identical 3D whole heart program steps are created in the workflow. The first step (1) is used only for monitoring the passage of contrast with the image navigator. The second step (2), which will run to completion, is triggered at the peak of the continuous infusion in the pulmonary artery. Inversion recovery gradient echo is also compatible with the 6000 Hz wideband pulse. **B** Depiction of the pulmonary vein ostial dimensions by double oblique multiplanar reformat technique

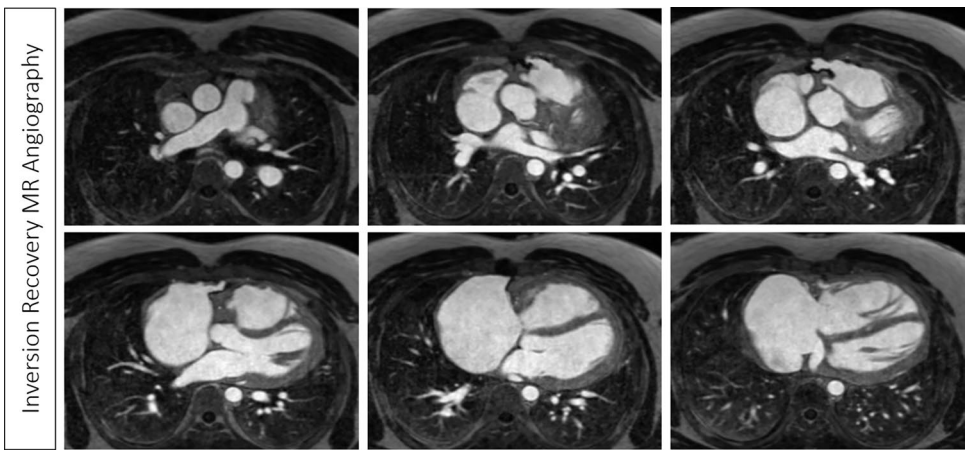

Fig. 4 Representative 3D images for pulmonary vein MR angiography with inversion recovery readout

CTA acquisition and ostial measurements

In order to provide a statistically meaningful analysis of pulmonary vein ostial dimensions between CTA and MRA, intended sample size exceeded that of previous research comparing iNAV developmental PV MRA to reference imaging [21]. CTA was performed on a 320-detector row scanner (Acquilion One, Vision, Canon Medical systems) with systolic-triggered cardiac gating at 45% RR interval. An automated bolus tracking region of interest (threshold of 100 Hounsfield units) centered in the left atrium was used, with delivery of 60 ml Omnipaque 350 at 4–5 ml/sec, followed by 30 ml saline at the same rate. Pulmonary vein major (maximum) and minor (minimum) ostial diameter measurements perpendicular to the vessel long axis were made using the double oblique MPR method and commercially available software (Vitrea®, Vital images for CTA; Syngo via®, Siemens Healthcare for MRI) by two independent, blinded cardiologists with 4 and 2 years of experience respectively (Fig. 3b). A total of 96 ostial measurements were obtained (4 pulmonary veins per patient, 2 dimensions per vein).

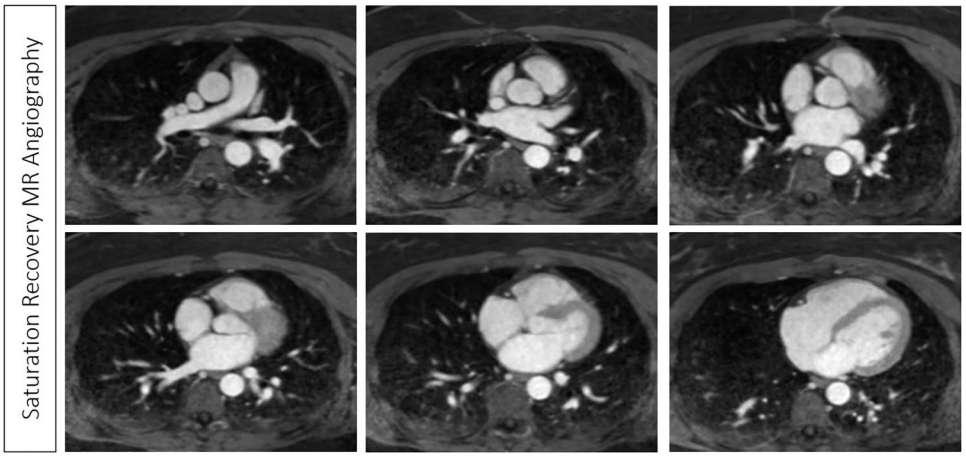

Fig. 5 Representative 3D images for pulmonary vein MR angiography with saturation recovery readout

Evaluation of study quality

Image and anatomical segmentation quality scoring was assessed based on a 4 point scale defined by Groarke, et al., who used DNAV based gated IR GRE PV MRA as the method of acquisition [22]. CE-MRA images were imported into electroanatomical mapping software (CartoMerge Image Integration Module, Biosense Webster Inc., Diamond Bar, CA USA). Segmentation of the left atrium, pulmonary veins and coronary sinus was performed using CartoMerge semi-automated image integration software, by two trained technologists with 11 years and 4 years of experience respectively. A total of 35 anatomical segmentations from 34 pre-afib ablation (PAFA) patients were completely redone independent of the pre-procedure anatomical segmentations and rated by each technologist blinded to the results of each other. One patient had both SR GRE and IR GRE 3D datasets because motion was suspected on the first (IR GRE) acquisition. However, both image sets were subsequently found to be free of patient motion. The remaining PAFA data sets consisted of 30 IR GRE exams, and 3 SR GRE exams.

Anatomical segmentation quality was graded on the following scale [22]: Grade 1: poor segmentation due to inability to separate LA and PVs from adjacent structures; Grade 2: moderate segmentation with incomplete separation of LA and PVs from adjacent structures; Grade 3: good segmentation with near complete separation of LA and PVs; Grade 4: excellent segmentation with complete separation of LA and PV.

Additionally, three cardiologists with 2 years, 2 years, and 5 years of experience respectively reviewed all datasets and rated image quality based on the following scale: 4- (excellent) excellent suppression of cardiac and/or respiratory motion, sufficient SNR; 3- (good) mild residual blurring of the pulmonary vessels (within 1 cm of the ostium) with sufficient SNR; 2- (poor) suboptimal SNR and/or motion suppression resulting in partially-diagnostic image; 1- (completely non-diagnostic image).

Statistical analysis

Continuous values and scores are reported as mean ± standard deviation, categorical values as frequency and percent. The inter-rater/intermodality reliability of ostial measurements, image, and anatomical segmentation quality were compared between board-certified imaging cardiologists, and two experienced technologists respectively. SNR/CNR, and quality scores between IR GRE vs SR GRE were compared using Wilcoxon's Rank-Score test and Fisher's exact test (for majority quality frequency). The reproducibility of the quality score was evaluated continuously and per score category through the use of the concordance correlation coefficient or Cohen's kappa with paired t-tests as appropriate, and presented using Bland–Altman plots. Interclass correlation coefficients (ICC), paired t-tests, as well as Bland–Altman plots and scatter plots with ordinary least squared regression lines were used to evaluate reproducibility of ostial measurements. Analyses were performed using SAS version 9.4 (Cary, NC.). Where applicable, p values of < 0.05 were considered statistically significant.

Results

Patient demographics

Patient demographics are given in Table 2. There were 18 (28%) patients who were in atrial fibrillation at the time of exam with a ventricular rate ranging from 54 to 102 bpm (mean 80 ± 12). This included 3 patients with chronic, 8 patients with paroxysmal, and 7 patients with persistent atrial fibrillation. For all patients, the overall heart rate ranged from 45 to 106 BPM (mean 70 ± 14) during image

Table 2 Patient demographics for the study population

Variable	Mean, N	SD, %
Age	67	13
Female gender (N, %)	26	40
Body mass index (kg/m^2)	30	6
Body surface area (m^2)	2.1	0.3
Heart rate (beats per minute)	70	14
Left atrial volume Index (mL/m^2)	57	25
Rhythm at time of MRA		
Normal sinus rhythm (N, %)	46	71
Atrial fibrillation (N, %)	18	28
Atrial fibrillation type (N)		
Chronic	3	
Paroxysmal	8	
Persistent	7	
Other rhythm (N, %)	1	2
Pacemaker device (N, %)	1	2
CHADS II VASC mean	2.8	1.8
CHADS II VASC frequency (N, %)		
0	6	9
1	12	18
2	12	18
3	15	23
4	6	9
5	9	14
6	5	8
Stroke/TIA (N, %)	6	9
Hypertension (N, %)	42	65
Coronary artery or peripheral vascular disease (N, %)	22	34
Diabetes (N, %)	12	18
NYHA heart failure class ≥ 2 (N, %)	10	15
Prior pulmonary vein isolation or atrial ablation (N, %)	17	26
Beta-blocker use (N, %)	45	69
Anti-arrhythmic use (N, %)	21	32
Valve disease (stenosis, regurgitation) ≥ mod-severe (N, %)	5	8

MRA magnetic resonance angiography; *CHADS II VASC* Congestive heart failure, Hypertension, Age, Diabetes, Stroke/transient ischemic attack (TIA), Vascular disease; *NYHA* New York Heart Association

acquisition. Mean BMI was 30 ± 6 kg/m^2. One patient had an implantable cardiac defibrillation, and one patient had a permanent pacemaker (Fig. 6).

Image quality assessment

Scan time for pulmonary vein iNAV 3D CE-MRA was 3.58 ± 0.60 min. All exams (66) were considered diagnostic. A total of 12 SR exams and 54 IR exams were included in the analysis. Image quality score data is presented in Table 3. Overall, the mean image quality score was 3.30 ± 0.58 as rated by physician 1, 3.59 ± 0.5 as rated by physician 2, and 3.71 ± 0.49 as rated by physician 3. The overall agreement (95% confidence limits) was 0.56 (0.40, 0.69) for physicians 1 and 2, 0.45 (0.23, 0.62) between physicians 2 and 3, and 0.32 (0.14, 0.48) between physicians 1 and 3. In total, 3 (2%) exams were rated as poor by the physician majority, with 62 (95%) exams receiving a majority score of good or excellent and 1 SR GRE (2%) exam which received entirely mixed scores (scored as poor, good, and excellent by the three physicians respectively). For patients in atrial fibrillation (systolic acquisition) versus normal sinus rhythm, mean image quality score was 3.05 ± 0.62 versus 3.40 ± 0.54 (p = 0.036) as rated by physician 1, 3.47 ± 0.51 versus 3.64 ± 0.49 (p = 0.2216) as rated by physician 2, and 3.63 ± 0.60 versus 3.74 ± 0.44 (p = 0.5457) as rated by physician 3. Mean image quality score for IR GRE vs SR

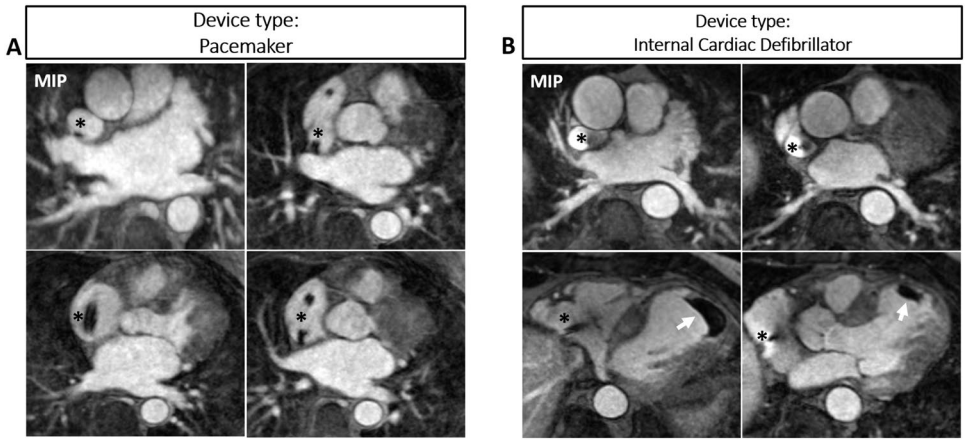

Fig. 6 Maximum intensity projection and multiplanar reformat wideband inversion recovery gradient echo images from two patients with cardiac devices. The intracardiac leads are denoted by asterisks. **A** Permanent pacemaker device type, and **B** internal cardiac defibrillator device type with incidentally discovered left ventricular thrombus (arrows)

Table 3 Image quality scores and agreement for all exams and comparisons between IR and SR GRE among physicians 1, 2, and 3

Overview of image quality scores				
Mean (SD) quality score	*All exams*	*IR*	*SR*	*p-value**
Physician 1	3.30 (0.58)	3.35 (0.55)	3.08 (0.67)	0.1885
Physician 2	3.59 (0.5)	3.65 (0.48)	3.33 (0.49)	0.0465
Physician 3	3.71 (0.49)	3.72 (0.49)	3.67 (0.49)	0.6363
Majority	3.52 (0.59)	3.56 (0.60)	3.36 (0.50)	0.2057
Agreement (95% limits)				
Physician 1 vs. 2	0.56 (0.40, 0.69)			
Physician 2 vs. 3	0.45 (0.23, 0.62)			
Physician 1 vs. 3	0.32 (0.14, 0.48)			
Majority quality, N (%)**				0.1558
Uninterpretable	0	0	0	
Poor	3 (5)	3 (6)	0	
Good	25 (38)	18 (33)	7 (64)	
Excellent	37 (57)	33 (61)	4 (36)	

*Inversion recovery (IR) vs saturation recovery (SR) mean quality score (Wilcoxon's Rank-score test) and majority quality frequency (Fisher's exact test)

**One SR exam had no majority quality score

GRE for all physicians is displayed in Table 3. Overall, mean image quality score was slightly better among IR exams, but this difference was only statistically significant for reviewer 2. Nineteen (33%) IR exams received a majority score of good, 33 (61%) received a majority score of excellent, and 3 (6%) received a majority score of poor. Seven (64%) of SR exams received a consensus score of good, 4 (36%) received as score of excellent, and 0 received a score of poor. A case rated as poor, primarily due to suboptimal rate control in atrial fibrillation is exemplified in supplemental_figure_1.pdf.

Measurement of SNR and CNR

The LA SNR and LA $CNR_{myocardium}$ ratios were 116.87 and 37.75 for the permanent pacemaker wideband IR GRE exam, and 228.73 and 103.27 for the implantable cardiac defibrillator wideband IR GRE exam respectively. The mean LA SNR for all IR GRE exams was 249.58 ± 190.58, with a LA $CNR_{myocardium}$ of 156.22 ± 128.11. For SR GRE, the mean LA SNR was 243.13 ± 125.52 with a LA $CNR_{myocardium}$ of 83.27 ± 47.73. There was no significant difference between IR GRE and SR GRE LA SNR ratios; whereas LA $CNR_{myocardium}$ was significantly higher for IR GRE (supplemental_figure_2.pdf).

Anatomical segmentation quality

Of the 35 pulmonary vein datasets (34 patients) used for ablation procedures, mean anatomical segmentation quality score was 3.66 ± 0.54 and 3.63 ± 0.55 as rated by technologists 1 and 2, respectively ($p = 0.7113$). Inter-rater agreement was 0.65 (0.40, 0.81). Technologist 1 scored 24 (69%) subjects as excellent, 10 (29%) as good, and 1 (3%) as moderate.

Technologist 2 scored 23 (66%) subjects as excellent, 11 (31%) as good, and 1 (3%) as moderate. Example MRA anatomical segmentations compared with CTA are provided in Fig. 7.

Ostial diameter comparison with CTA

Interobserver and intermodality comparisons between major and minor ostial dimensions are reported in Table 4 and Fig. 8. Regression analysis plots can be found in supplemental_figure_3.pdf. The interobserver comparisons of CTA major/minor ostia dimensions had a mean difference of 0.22 ± 3.28 mm ($p = 0.66$) and 0.64 ± 2.43 mm ($p = 0.081$), respectively, and 1.44 ± 3.33 mm ($p = 0.005$) and 2.47 ± 2.83 mm ($p = 0.001$) for MRA with reflecting ICC values suggesting better reproducibility on CTA. The intermodality comparisons within reader 1 was -0.2 ± 2.28 mm ($p = 0.55$) and -0.61 ± 3.3 mm ($p = 0.23$) for major/minor

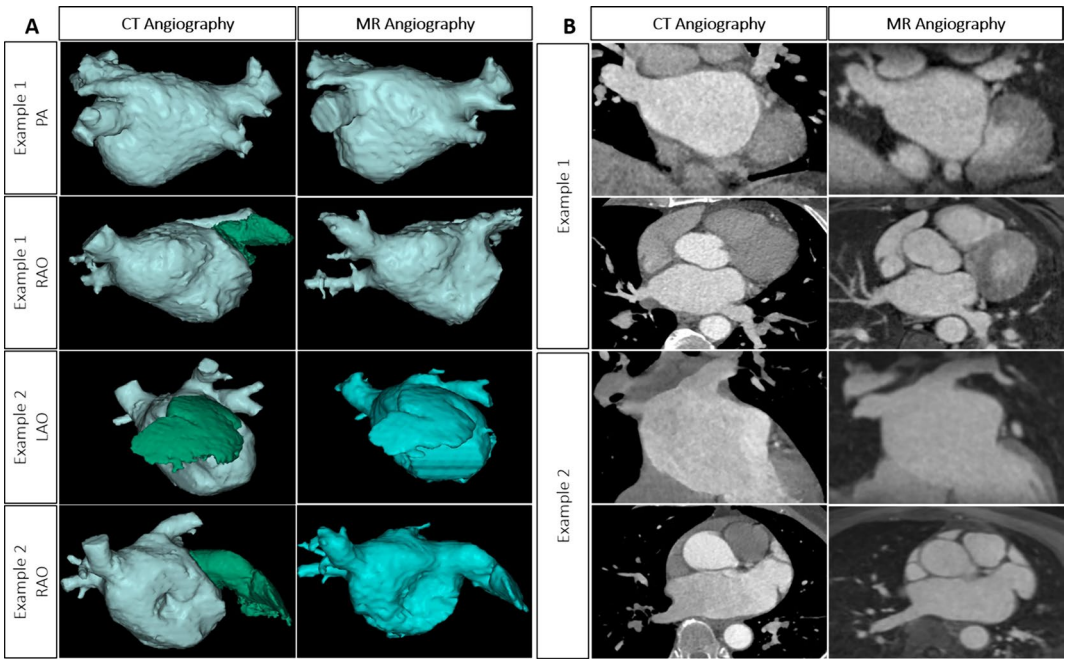

Fig. 7 Example comparison between CT and MR angiography segmentations of the left atrium and pulmonary veins

Table 4 Intermodality and interobserver comparison between major and minor ostia dimensions performed on CTA and MRA

	Intermodality comparison					
	Dimension*	CTA mean	MRA mean	Mean difference	p-value**	ICC
Reader 1	Major	19.5 ± 3.56	19.7 ± 3.3	-0.2 ± 2.28	0.55	0.78 (0.63, 0.87)
	Minor	15.62 ± 3.79	16.23 ± 2.98	-0.61 ± 3.3	0.23	0.52 (0.28, 0.7)
	Quality	3.42 ± 0.51	3.33 ± 0.49	0.08 ± 0.79	0.72	
Reader 2	Major	19.28 ± 4.53	18.26 ± 4.3	1.02 ± 2.09	0.002	0.86 (0.77, 0.92)
	Minor	14.98 ± 4.43	13.76 ± 3.68	1.22 ± 2.41	0.001	0.79 (0.66, 0.87)
	Interobserver comparison					
	Dimension	Reader 1 mean	Reader 2 mean	Mean difference	p-value	ICC
CTA	Major	19.5 ± 3.56	19.28 ± 4.53	0.22 ± 3.28	0.66	0.67 (0.49, 0.8)
	Minor	15.62 ± 3.79	14.98 ± 4.43	0.64 ± 2.43	0.081	0.82 (0.69, 0.89)
MRA	Major	19.7 ± 3.3	18.26 ± 4.3	1.44 ± 3.33	0.005	0.58 (0.37, 0.73)
	Minor	16.23 ± 2.98	13.76 ± 3.68	2.47 ± 2.83	0.001	0.51 (0.31, 0.66)

CTA computed tomography angiography; *MRA* magnetic resonance angiography

*All ostia dimensions are measured in millimeters

**Comparisons were performed using paired t-tests or Signed rank test as appropriate

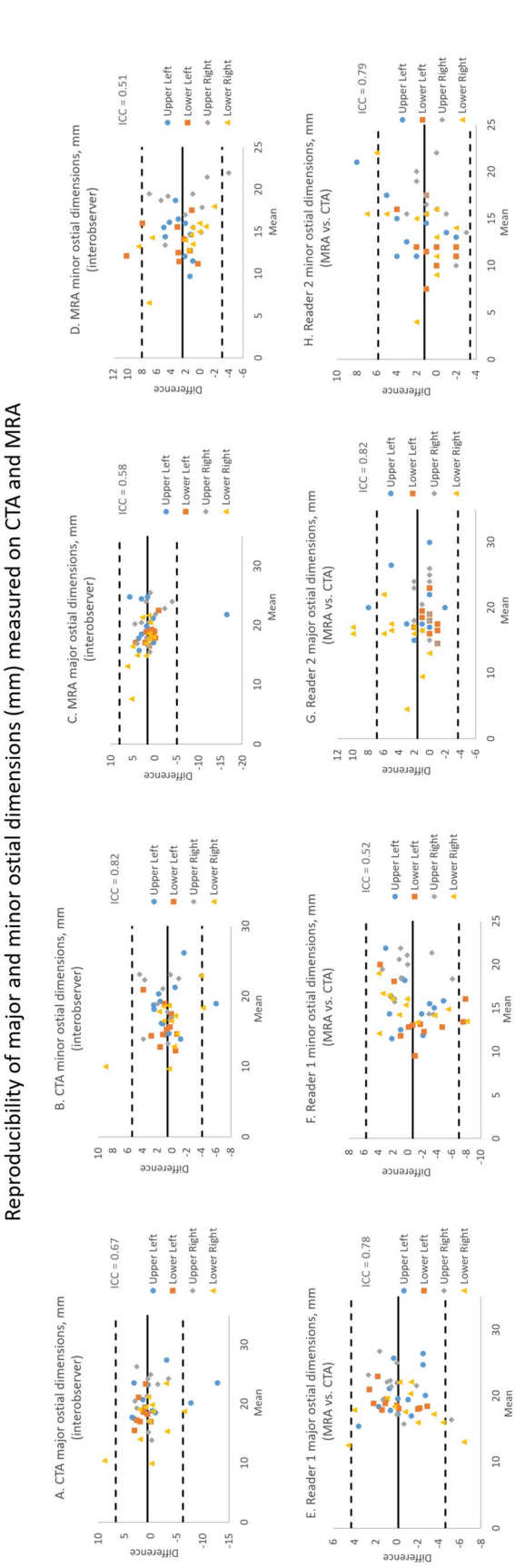

Fig. 8 Bland–Altman plots demonstrating interobserver reproducibility of CTA major (**A**), minor (**B**) ostial dimensions, MRA major (**C**), minor (**D**) ostial dimensions, as well as intermodality reproducibility comparing MRA and CTA major and minor dimensions by reader 1 (**E** and **F**) and reader 2 (**G** and **H**)

dimensions, respectively, and 1.02 ± 2.09 mm (p = 0.002) and 1.22 ± 2.41 mm (p = 0.001) for reader 2. The mean CTA radiation dose was 2.01 ± 0.47 mSv.

Discussion

In this study, good to excellent PV iNAV 3D CE-MRA image quality and high quality anatomical segmentation was achieved in 95% and 97% of patients respectively by using iNAV fluoro triggering combined with previously described iNAV VD-CASPR for motion corrected whole heart 3D imaging [17]. Although adequate for pre-ablation imaging, a potential barrier to the use of gated MRA for pre-ablation imaging has been prolonged acquisition times and complexity compared to CTA. In this work, we have satisfied the aim of providing a simplified injection scheme practical for everyday clinical use without contrast dilution, manipulation of extra tubing and/or stop cocks [23, 24]; and imaging was completed in under 4 min. We have been inspired by previous works in the field using dNAV, and most recently iNAV to provide clinicians with motion corrected high-resolution gated MRA [24, 25]. Compared to this previous studies with protocols designed for whole chest MRA, we used a smaller bolus dose of 0.05 mmol/kg, which provides adequate background signal for iNAV tracking. iNAV could allow for potentially smaller GBCA doses due to the following: precision timing of scan initiation at the peak of the continuous infusion using the fluoro-trigger method; and improved robustness to respiratory motion and 100% scan efficiency by directly tracking the left ventricular blood pool rather than the diaphragm. Additionally, the increased scan efficiency can be traded for higher spatial resolution, assuming SNR adequacy is maintained.

We also used two different preparations schemes- SR GRE and IR GRE. Sheffer et al. first described use of SR GRE for pulmonary vein imaging at 3 T [3] and found this method less sensitive to RR variation compared to first pass MRA for patients in atrial fibrillation. Saturation times of 150 and 250 ms have been described [26]. SR GRE has the perceived advantage of consistent image contrast despite RR interval variation; however, it is our observation that IR GRE image contrast fidelity was overall maintained regardless of sinus rhythm. Based on a limited number of SR GRE exams, we found no significant difference in LA SNR compared to IR GRE; conversely, LA $CNR_{myocardium}$ was higher in the IR GRE group. A further comparison of image quality, vessel sharpness, CNR, and SNR may be the subject of investigation given the small size of our SR GRE cohort.

The TI selection for IR GRE was a balance between SNR and background tissue suppression, and was generally longer than the value used by Groarke et al. (200 ms) for PV CE-MRA [22]. However, there still was an adequate amount of background tissue signal intensity suppression. This largely eliminated the need for fat saturation preparatory pulses which may lead to inadvertent water saturation. In comparison, fat suppression combined with SR GRE is mandatory to reduce artifacts and to suppress background signal. It is estimated that approximately 50–100 Hz off-resonance is frequently observed at the interface of the pulmonary veins and left atrium due to susceptibility effects and inflow from the lungs [4]. Accordingly, use of bSSFP readouts could be problematic resulting in signal inhomogeneity, poorer visualization of the proximal pulmonary veins, and more laborious threshold- based segmentations. Although radial, self NAV 3D bSSFP has been shown to significantly reduce blood pool inhomogeneity artifacts in other anatomical regions compared to the standard Cartesian readout [27], it has yet to be demonstrated whether this method can provide artifact free imaging of the pulmonary veins. Furthermore, radial readouts do not eliminate bSSFP flow artifacts in this region [28]. Lastly, a 6000 Hz wideband IR pulse in conjunction with a + 1500 Hz center frequency offset facilitated use in patients with an internal defibrillator or pacemaker device respectively.

We decided not to exclude patients in atrial fibrillation for our comparison with CTA. Although only 4 out of 12 patients in the CTA comparison group were in atrial fibrillation at the time of MRA, the inclusion of these patients is more relevant to everyday clinical practice. Compared to Hamdan et al. [29] and Fahlenkamp et al. [30], who exclusively imaged patients in sinus rhythm, we found lower intermodality agreement between CTA and MRA ostial pulmonary vein measurements.. These differences may possibly be explained by the larger sample sizes of the aforementioned studies and our inclusion of patients in atrial fibrillation. Residual ostial blurring due to cardiac motion may be observed in patients with irregular rhythms. Despite this, the mean differences in PV ostial measurements were at most 1.2 mm between the two modalities, which is comparable to Hamdan et al.

Limitations

There are limitations to the current study that could be addressed with additional research. A small number of patients received CTA imaging for comparison, in part, due to iodinated contrast shortages. Additionally, we did not obtain first pass MRA for a comparison reference. As such, we are not able to establish our method for PV MRA as superior to ungated first pass CE-MRA in terms of image/anatomical segmentation quality or reproducibility of PV ostial measurements. As mentioned, one patient had an interim PVI between imaging studies. Although a reduction in pulmonary vein ostial size may be expected 3 months

post-PVI [31] (approximately 10%), little data exist regarding persistent of these changes in the absence of pulmonary vein stenosis.

Conclusion

Cardiac gated PV CE-MRA can be obtained in under 4 min using iNAV based 3D IR GRE or SR GRE cardiac imaging. The approach of using the iNAV as a (1) fluoro trigger and (2) 100% respiratory efficient PV CE-MRA with variable density sampling with non-rigid motion corrected reconstruction allows for precision scan timing in relation to the contrast infusion and high quality MRA.

Supplementary Information The online version contains supplementary material available at https://doi.org/10.1007/s10554-024-03111-0.

Acknowledgements Drs Eddy Barasch, Haoyi Zheng, Lu Chen, Lin Wang, Praveena Paruchuri, Dennis Mihalatos, Kathleen Stergiopoulos, Jane Cao, and Kana Fujikura for providing clinical support. Dr Orlando Simonetti for his feedback on submission quality.

Author Contributions JC- manuscript lead/main author, study design (MR parameters, MR protocol, injection protocol, post-processing), supervising physician. JW/JAR/LF/CBE-statistical analysis, preparations of chart/tables. YL-preparation of figures. SW- project management, patient recruitment, nursing supervisor. MG- project management, project coordination, patient recruitment, data management. CP/RMB/KPK/RN/MS- sequence concept and design, physicist level support of project. RMB and CP substantially contributed to the revision of the manuscript. JT- data management, project management, database design. EH-protocol preparation, project management, project coordination. RP-expert opinion on image quality. AO- expert opinion on image quality, ostial measurements. OKK- expert opinion on image quality. KF-expert opinion on image quality, ostial measurements. MC-expert opinion on segmentation quality. DF- expert opinion on segmentation quality. JYC- patient management, chief MR operator, MR protocol design and implementation, MR supervision. ND/AY-patient management, MR operator, protocol training and MR supervision. All authors participated in manuscript revision. All authors read and approved the final manuscript.

Declarations

Funding This manuscript was funded by an endowment from the St. Francis Hospital Foundation.

Competing interests MG/EH/ND/JYC/SW/JW/AO/RP/JT/AY/OKK/CP/RMB/JAR/CBE/LF/KF have no competing interest.

Financial interests OKK has no disclosures relevant to contents of this manuscript. General disclosures: consultant, Edwards Lifesciences, Croivalve, Philips Healthcare, Cardiac Implants, Restore Medical. Equity, Cardiac Implants, Triflo. JTC has no disclosures relevant to the contents of this manuscript. General disclosures: honorarium from Philips Healthcare. MS, KPK and RN are employees of Siemens Healthcare MC and DF are employees of Biosense Webster Incorporated.

Ethics approval The study protocol was approved by the Saint Francis Hospital IRB, Roslyn NY as reference # 19–27.

Consent to participate Informed consent, or waiver of informed consent was provided for each MRA exam.

Consent to publish The authors affirm that human research participants provided informed consent for publication of the images in Figs. 3 , 4, 5, 6 and 7.

References

1. Amukotuwa SA, Bammer R, Jackson DM, Sutherland T (2022) Iodinated contrast media shortage: insights and guidance from two major public hospitals. J Med Imaging Radiat Oncol 66:946–956. https://doi.org/10.1111/1754-9485.13444
2. Dong J, Dickfeld T, Dalal D, Cheema A, Vasamreddy CR, Henrikson CA, Marine JE et al (2006) Initial experience in the use of integrated electroanatomic mapping with three-dimensional MR/CT images to guide catheter ablation of atrial fibrillation. J Cardiovasc Electrophysiol 17:459–466. https://doi.org/10.1111/j.1540-8167.2006.00425.x
3. Sheffer D, Kholmovski E, Chang L, Velagapudi KN, Damal K, Marrouche NF, McGann C (2013) Improved left atrial imaging in atrial fibrillation patients using novel ECG-gated vs. conventional non-gated cardiac MRA. J Cardiovasc Magn Reson 15:O50. https://doi.org/10.1186/1532-429X-15-S1-O50
4. Hu P, Peters DC, Stoeck C, Kissinger KV, Goddu B, Goepfert L, Manning WJ et al (2009) Off-resonant pulmonary vein imaging. J Cardiovasc Magn Reson. https://doi.org/10.1186/1532-429X-11-S1-P185
5. Rashid I, Ginami G, Nordio G, Fotaki A, Neji R, Alam H, Pushparajah K, Frigiola A, Valverde I, Botnar RM, Prieto C (2023) Magnetization transfer BOOST noncontrast angiography improves pulmonary vein imaging in adults with congenital heart disease. J Magn Reson Imaging 57(2):521–531. https://doi.org/10.1002/jmri.28280
6. Pennig L, Wagner A, Weiss K, Lennartz S, Grunz J-P, Maintz D, Laukamp KR et al (2020) Imaging of the pulmonary vasculature in congenital heart disease without gadolinium contrast: intraindividual comparison of a novel compressed SENSE accelerated 3D modified REACT with 4D contrast-enhanced magnetic resonance angiography. J Cardiovasc Magn Reson 22:8. https://doi.org/10.1186/s12968-019-0591-y
7. von Knobelsdorff-Brenkenhoff F, Gruettner H, Trauzeddel RF, Greiser A, Schulz-Menger J (2014) Comparison of native high-resolution 3D and contrast-enhanced MR angiography for assessing the thoracic aorta. Eur Heart J Cardiovasc Imaging 15:651–658. https://doi.org/10.1093/ehjci/jet263
8. Kawaji K, Spincemaille P, Nguyen TD, Thimmappa N, Cooper MA, Prince MR, Wang Y (2014) Direct coronary motion extraction from a 2D fat image navigator for prospectively gated coronary MR angiography. Magn Reson Med 71:599–607. https://doi.org/10.1002/mrm.24698
9. Addy NO, Ingle RR, Luo J, Baron CA, Yang PC, Hu BS, Nishimura DG (2017) 3D image-based navigators for coronary MR angiography. Magn Reson Med 77:1874–1883. https://doi.org/10.1002/mrm.26269
10. Moghari MH, Roujol S, Chan RH, Hong SN, Bello N, Henningsson M, Ngo LH et al (2013) Free-breathing 3D cardiac MRI using iterative image-based respiratory motion correction. Magn Reson Med 70:1005–1015. https://doi.org/10.1002/mrm.24538
11. Keegan J, Gatehouse PD, Yang G-Z, Firmin DN (2007) Non-model-based correction of respiratory motion using beat-to-beat 3D spiral fat-selective imaging. J Magn Reson Imaging 26:624–629. https://doi.org/10.1002/jmri.20941

12. Henningsson M, Koken P, Stehning C, Razavi R, Prieto C, Botnar RM (2012) Whole-heart coronary MR angiography with 2D self-navigated image reconstruction. Magn Reson Med 67:437–445. https://doi.org/10.1002/mrm.23027
13. Bustin A, Ginami G, Cruz G, Correia T, Ismail TF, Rashid I, Neji R et al (2019) Five-minute whole-heart coronary MRA with sub-millimeter isotropic resolution, 100% respiratory scan efficiency, and 3D-PROST reconstruction. Magn Reson Med 81:102–115. https://doi.org/10.1002/mrm.27354
14. Zeilinger MG, Kunze K-P, Munoz C, Neji R, Schmidt M, Croisille P, Heiss R et al (2022) Non-rigid motion-corrected free-breathing 3D myocardial dixon LGE imaging in a clinical setting. Eur Radiol 32:4340–4351. https://doi.org/10.1007/s00330-022-08560-6
15. Hajhosseiny R, Rashid I, Bustin A, Munoz C, Cruz G, Nazir MS, Grigoryan K et al (2021) Clinical comparison of sub-mm high-resolution non-contrast coronary CMR angiography against coronary CT angiography in patients with low-intermediate risk of coronary artery disease: a single center trial. J Cardiovasc Magn Reson 23:57. https://doi.org/10.1186/s12968-021-00758-9
16. Fotaki A, Munoz C, Emanuel Y, Hua A, Bosio F, Kunze KP, Neji R et al (2022) Efficient non-contrast enhanced 3D Cartesian cardiovascular magnetic resonance angiography of the thoracic aorta in 3 min. J Cardiovasc Magn Reson 24:5. https://doi.org/10.1186/s12968-021-00839-9
17. Munoz C, Bustin A, Neji R, Kunze KP, Forman C, Schmidt M, Hajhosseiny R et al (2020) Motion-corrected 3D whole-heart water-fat high-resolution late gadolinium enhancement cardiovascular magnetic resonance imaging. J Cardiovasc Magn Reson 22:53. https://doi.org/10.1186/s12968-020-00649-5
18. Tandon A, Hashemi S, Parks WJ, Kelleman MS, Sallee D, Slesnick TC (2016) Improved high-resolution pediatric vascular cardiovascular magnetic resonance with gadofosveset-enhanced 3D respiratory navigated, inversion recovery prepared gradient echo readout imaging compared to 3D balanced steady-state free precession readout imaging. J Cardiovasc Magn Reson 18(1):74. https://doi.org/10.1186/s12968-016-0296-4
19. Zheng J, Bae KT, Woodard PK, Haacke EM, Li D (1999) Efficacy of slow infusion of gadolinium contrast agent in three-dimensional MR coronary artery imaging. J Magn Reson Imaging 10(5):800–805. https://doi.org/10.1002/(sici)1522-2586(199911)10:5%3c800::aid-jmri26%3e3.0.co;2-l
20. Rashid S, Rapacchi S, Shivkumar K, Plotnik A, Finn JP, Hu P (2016) Modified wideband three-dimensional late gadolinium enhancement MRI for patients with implantable cardiac devices. Magn Reson Med 75(2):572–584. https://doi.org/10.1002/mrm.25601
21. Ginami G, Lòpez K, Mukherjee RK, Neji R, Munoz C, Roujol S, Mountney P et al (2019) Non-contrast enhanced simultaneous 3D whole-heart bright-blood pulmonary veins visualization and black-blood quantification of atrial wall thickness. Magn Reson Med 81:1066–1079. https://doi.org/10.1002/mrm.27472
22. Groarke JD, Waller AH, Vita TS, Michaud GF, Di Carli MF, Blankstein R, Kwong RY et al (2014) Feasibility study of electrocardiographic and respiratory gated, gadolinium enhanced magnetic resonance angiography of pulmonary veins and the impact of heart rate and rhythm on study quality. J Cardiovasc Magn Reson 16:43. https://doi.org/10.1186/1532-429X-16-43
23. Lam CZ, Pagano JJ, Gill N, Vidarsson L, de la Mora R, Seed M, Grosse-Wortmann L et al (2019) Dual phase infusion with bolus tracking: technical innovation for cardiac and respiratory navigated magnetic resonance angiography using extracellular contrast. Pediatr Radiol 49:399–406. https://doi.org/10.1007/s00247-018-4293-7
24. Tandon A, James L, Henningsson M, Botnar RM, Potersnak A, Greil GF, Hussain T (2016) A clinical combined gadobutrol bolus and slow infusion protocol enabling angiography, inversion recovery whole heart, and late gadolinium enhancement imaging in a single study. J Cardiovasc Magn Reson 18:66. https://doi.org/10.1186/s12968-016-0285-7
25. Dabir D, Naehle CP, Clauberg R, Gieseke J, Schild HH, Thomas D (2012) High-resolution motion compensated MRA in patients with congenital heart disease using extracellular contrast agent at 3 tesla. J Cardiovasc Magn Reson 14:75. https://doi.org/10.1186/1532-429X-14-75
26. Siebermair J, Kholmovski EG, Sheffer D, Schroeder J, Jensen L, Kheirkhahan M, Baher AA et al (2021) Saturation recovery-prepared magnetic resonance angiography for assessment of left atrial and esophageal anatomy. Br J Radiol 94:20210048. https://doi.org/10.1259/bjr.20210048
27. Heerfordt J, Stuber M, Maillot A, Bianchi V, Piccini D (2020) A quantitative comparison between a navigated cartesian and a self-navigated radial protocol from clinical studies for free-breathing 3D whole-heart bSSFP coronary MRA. Magn Reson Med 84(1):157–169. https://doi.org/10.1002/mrm.28101
28. Robb JS, Hu C, Peters DC (2020) Interleaved, undersampled radial multiple-acquisition steady-state free precession for improved left atrial cine imaging. Magn Reson Med 83(5):1721–1729. https://doi.org/10.1002/mrm.28036
29. Hamdan A, Charalampos K, Roettgen R, Wellnhofer E, Gebker R, Paetsch I, Jahnke C et al (2009) Magnetic resonance imaging versus computed tomography for characterization of pulmonary vein morphology before radiofrequency catheter ablation of atrial fibrillation. Am J Cardiol 104:1540–1546. https://doi.org/10.1016/j.amjcard.2009.07.029
30. Fahlenkamp UL, Lembcke A, Roesler R, Schwenke C, Huppertz A, Streitparth F, Taupitz M, Hamm B, Wagner M (2013) ECG-gated imaging of the left atrium and pulmonary veins: intra-individual comparison of CTA and MRA. Clin Radiol 68(10):1059–1064. https://doi.org/10.1016/j.crad.2013.05.006
31. Gottlieb LA, Al Jefairi N, El Hamrani D, Naulin J, Lamy J, Kachenoura N, Constantin M et al (2021) Reduction in left atrial and pulmonary vein dimensions after ablation therapy is mediated by scar. Int J Cardiol Heart Vasc 37:100894. https://doi.org/10.1016/j.ijcha.2021.100894